Nanostructured Single Crystals Sandwiched between Ordered/Disordered Coily and Rod Brushes

Agbolaghi, Samira*[+]

Chemical Engineering Department, Faculty of Engineering, Azarbaijan Shahid Madani University, Tabriz, I.R. IRAN

Abbaspoor, Saleheh

Institute of Polymeric Materials, Sahand University of Technology, Tabriz, I.R. IRAN

Alizadeh-Osguei, Mona

School of Aerospace, Mechanical and Manufacturing Engineering, RMIT University, Melbourne, AUSTRALIA

Nazari, Maryam

Department of Chemistry, University of Calgary, Calgary, CANADA

Abbasi, Farhang

Institute of Polymeric Materials, Sahand University of Technology, Tabriz, I.R. IRAN

ABSTRACT: *Single crystals of poly(ethylene glycol) (PEG)-b-polystyrene (PS), PEG-b-poly(methyl methacrylate) (PMMA), PEG-b-polycaprolactone (PCL), and polyaniline (PANI)-b-PEG-b-PANI were developed from dilute solutions and thin molten films using self-seeding methodology. The PS and PMMA grafted chains were categorized in disordered nano-brushes; however, the PCL and PANI ones were grouped in ordered nano-brushes. The characteristics of grown single crystals such as surface morphology, growth planes, and thicknesses were investigated using Atomic Force Microscopy (AFM), Electron Diffraction (ED) in Transmission Electron Microscopy (TEM), and Small Angle X-ray Scattering (SAXS). The thickness of PEG substrates, as well as polymer nano-brushes, were in the nanoscale (2-150 nm). Furthermore, the special morphologies of polymer mixed-brushes developed through the growth of single crystals of PEG-b-PS and PEG-b-PMMA diblock copolymers were introduced and characterized. Regardless of different morphologies, the total, substrate and amorphous thicknesses, tethering density as well as ED patterns were compatible in the phase regions covered by similar nano-brushes.*

KEYWORDS: *Disordered/ordered; Nano-brush; Self-seeding; Single crystal; Morphology.*

INTRODUCTION

Polymer single crystals (PSCs) have shown numerous applications, e.g., PSC growth directed programmable

* *To whom correspondence should be addressed.*

+ E-mail: chemeng96sa1987@yahoo.com

1021-9986/2018/4/15-25 11/$/6.01

assembly of nanoparticles [1], nano-hybrid shish-kebabs to mimic the natural bone nanostructures [2], magnetically recyclable catalyst support [3-7], templates to synthesize nanoparticle clusters [8,9], substrates for anisotropic deposition of Au nanoparticles [10], utilizable in semiconductor microelectronics and solid-state [11,12], simplified ultrathin film system to probe the interfacial properties of different substrates [13], the amino-functionalized lamellar poly(L-lactide) single crystals as a delivery system for human papillomaviruses (HPV16-E7) -associated tumors [14-16], nano/micromotors [17,18], etc. In the conductive materials field, large single rectangular crystals of the regioregular octamer of 3-hexyl-thiophene $(3HT)_8$ [19,20], well-defined single crystalline nanowires of rigid rod conjugated poly(*p*-phenylene ethynylene) derivatives with thioacetate end groups (TA-PPE) [21], single nano-whiskers of poly(3-hexylthiophene) (P3HT) [22], one dimensional (1D) microwire single crystals of P3HT (regioregularity = 98.5%) [12,23], self-organized P3HT with its supramolecular two dimensional (2D) structure [24,25], poly(3-octylthiophene) (P3OT) single crystals through solvent vapor annealing process [26], etc were reported.

Polymer brushes having high sensitivity to environmental alterations could be employed in many applications such as biomaterials, microfluidic devices, tissue engineering, membrane surface modification, colloidal stabilization, chemical sensors, and ion-exchange adsorbents [27-31]. A surface-grafted monolayer having a combination of various properties is obtainable via fabrication of the polymer mixed-brushes. It is noteworthy that due to the presence of different polymer brushes with various behaviors in mixed-brush structures, they are capable of introducing a wide range of morphologies and responses [32,33]. To construct mixed-brushes, various methods such as grafting to [34-36], grafting from [37-41], a combination of these approaches, single crystal growth of block copolymers [42], and patterning of single crystal surface [43-50] have been previously presented.

In the current work, the highly crystalline PEG structures covered by the hairy or nano-brush regions with rod and coily configurations have been investigated from the perspective of dimensions, surface patterning, ordering, and brush conformation by SAXS, AFM, and SAED TEM analyses.

EXPERIMENTAL SECTION

The PEG-b-PS, PEG-b-PMMA, PANI-b-PEG-b-PANI, and PEG-b- PCL block copolymers were synthesized via Atom Transfer Radical Polymerization (ATRP), interfacial polymerization, and ring opening polymerization [43,47]. To fabricate the single crystals of crystalline-amorphous block copolymers, the self-seeding method was utilized [51,52]. In brief, a solution crystallization was carried out with a dilute concentration of 0.009 wt % of solute in amyl acetate. The sample was put into a cell tube containing solvent, and heated above the dissolution temperature of the sample in the solvent in a temperature-controllable oil bath and kept for about 10-15 minutes; subsequently, the cell tube containing sample and solvent was transferred to another bath at present crystallization temperature which was appropriately below the room temperature, lasting 5-6 hours for fast crystallization, and then immersed into a given self-seeding temperature oil bath (T_s = 41 ºC for all samples), and kept for 20 min. The cell tube in question was then quickly switched into an isothermal oil bath with desired crystallization temperature (23-32 °C) and maintained for 2-3 days.

The chemical structure of block copolymers was confirmed by ^{1}HNMR spectroscopy on a Bruker (Avance DPX) spectrometer working at 400 MHz. The characteristics of single crystals were investigated by AFM, Nanoscope III in the tapping mode, transmission electron microscope (TEM, EM 208 Philips) equipped with Selected Area Electron Diffraction (SAED) facility, and Bruker-AXS Nanostar SAXS with a counts rate of 1000 s/sec/channel and spatial resolution of 400-500 µm.

RESULTS AND DISCUSSIONS

In the current work, we developed distinct types of single crystalline grained structures at different temperatures and preparation conditions using PEG-*b*-PS, PEG-*b*-PMMA, PANI-*b*-PEG-*b*-PANI, and PEG-*b*-PCL block copolymers. The PANI nanorods were rigid and rod, the PS nano-brushes were extended coily, the PMMA nano-brushes were packed coily, and PCL nano-brushes were ordered on the PEG crystalline substrates. By mixing the coily brushes of PS and PMMA, various surface morphologies were also detected for the developed grained nanostructures.

Disordered coily brush-covered nanostructured single crystals

The particular morphologies detected in growth systems of mixed-brush single crystals were categorized into some species: disperses in snake-, ring-, and dumbbell-shape formed from PMMA brushes in PS-matrix, patched surface areas covered by PS and PMMA grafted chains and random channel-like morphologies with alternative channels constructed from two different phases. Amyl acetate was a very good solvent for PS blocks and a partially poor solvent for PMMA blocks [53]. The PS tethered chains had repulsive interaction with the corresponding substrate surface [4], thereby, detection of the different phase regions covered with extended PS and partially packed pancake PMMA tethered chains was feasible on the substrate. Figs. 1(a) and (b) depict AFM height and phase images of matrix (PS)-dispersed (PMMA) surface morphology of PEG_{5000}-*b*-PS_{4600}/PEG_{5000}-*b*-$PMMA_{17100}$ grown at T_c = 30 °C, respectively. The height variance and average domain sizes were 2.70 and 303 nm, respectively. These parameters were 1.89 and 302 nm at T_c = 23 °C. This type of arrangement for the coily PS and PMMA brushes was attributed to their conformations originated from the solvent quality and interaction with the single crystalline substrate. Fig. 1(c) illustrates ring-like surface morphology of PEG_{5000}-*b*-PS_{4600}/PEG_{5000}-*b*-$PMMA_{8700}$ grown at T_c = 32 °C having a height variance of 4.90 nm. It is noteworthy that the corresponding sample possessing leopard skin-like morphology demonstrated a height variance of 4.88 nm. Hence, regardless of fabricated morphologies, the height variances were highly compatible with each other. Fig. 1(d) shows the patched surface morphology for PEG_{5000}-*b*-PS_{4600}/PEG_{5000}-*b*-$PMMA_{13100}$ single crystal grown at T_c = 30 °C, in which the height variance between the PS- and PMMA-covered phases was 3.62 nm. Figs. 1(e) and (f) present narrow channel-wire surface morphology of PEG_{5000}-*b*-PS_{10000}/PEG_{5000}-*b*-$PMMA_{17100}$ single crystal grown at T_c = 30 °C (height variance = 4.80 nm) and broad channel-wire surface morphology of PEG_{5000}-*b*-PS_{10000}/PEG_{5000}-*b*-$PMMA_{13100}$ single crystal grown at T_c = 23 °C (height variance = 5.22 nm), respectively. In a constant molecular weight of PS brushes, i.e., 10000 g/mol, via enhancing the molecular weight of PMMA tethered chains from 13100 to 17100 g/mol, the width of channels decreased. Distinct crystallization temperatures (23 and 30 °C) did not affect the domain size and shape.

The constructed mixed-brush surface morphologies were not in the request of any selective solvent to be detected. Regarding the density variance and different hardness of the PMMA and PS amorphous blocks [54], detection of phase regions on the single crystal substrate was possible. In addition to the mentioned parameters, thanks to different qualities of applied solvent in growth conditions for PS brushes, we were able to investigate the height variances. Furthermore, the type of interaction of different tethered chains with substrate surface (repulsive and attractive for PS and PMMA tethered chains, respectively) could, in turn, be considered as the most effective parameter on detection of phase regions.

The tethering density (the number of tethered chains in a unit area of the surface [55]) and crystalline substrate thickness were determined based on Equations (1) and (2), respectively [3,4].

$$\sigma = \frac{1}{S} = \frac{1}{\frac{2M_n^{CRYST}}{N_A \rho_{CRYST} d_{CRYST}}} = \frac{N_A \rho_{CRYST} d_{CRYST}}{2M_n^{CRYST}} \quad (1)$$

$$d_{CRYST} = d^{total} \times \frac{M_n^{CRYST} / \rho_{CRYST}}{M_n^{CRYST} / \rho_{CRYST} + M_n^{AM} / \rho_{AM}} \quad (2)$$

Where σ, N_A, ρ_{CRYST}, d_{CRYST}, M_n^{CRYST}, d^{total}, M_n^{AM}, and ρ_{AM} stood for the tethering density, Avogadro number (= 6.022×10^{23} mol^{-1}), crystalline PEG density (1.239 g/cm^3 at room temperature) [56], PEG substrate thickness (Equation (2)), molecular weight of PEG (5000 g/cm^3 for all samples), total thickness, molecular weight of amorphous blocks, density of amorphous blocks (1.19 g/cm^3 [53] for PMMA and 1.05 g/cm^3 [56] for PS), respectively.

Through conducting AFM analyses with more scrutiny on various samples, and comparing achieved height profiles, it was clear that irrespective of shape and size of areas covered by PMMA brushes in PS-matrix, the total, substrate, and amorphous brushes thickness were similar in different morphologies for a given molecular weight of tethered chains. In Figs. 2(a) and (b), AFM height images of snake-like and matrix-dispersed surface morphologies are demonstrated for mixed-brush single crystals of PEG_{5000}-*b*-PS_{14800}/PEG_{5000}-*b*-$PMMA_{17100}$

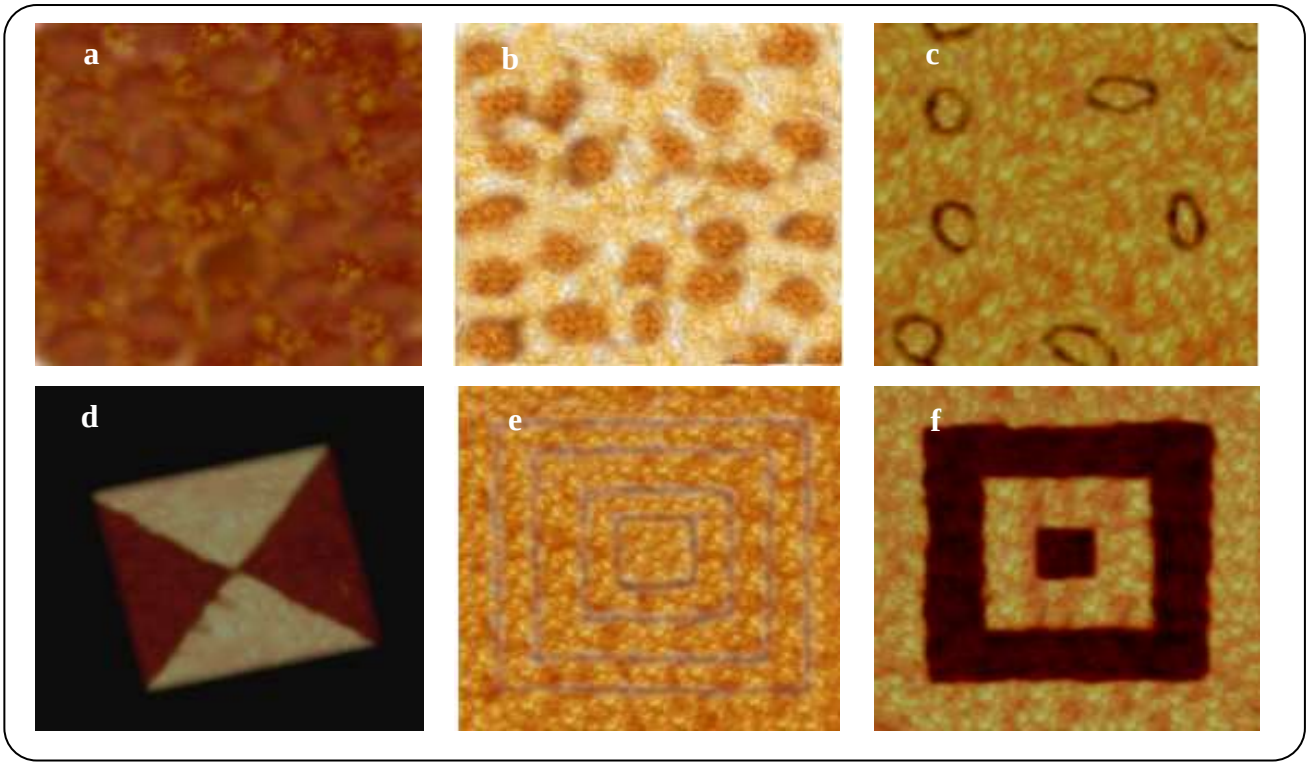

Fig. 1: AFM Nanoscope images of mixed-brush single crystals. The height image of matrix (PS)-dispersed (PMMA) surface morphology of PEG_{5000}-b-PS_{4600}/PEG_{5000}-b-$PMMA_{17100}$ grown at T_c = 30 °C (the maximum z-scale is 5 nm), height variance: 2.70 nm, domain size: 303 nm (a) continued by respective phase image (b); ring-like surface morphology of PEG_{5000}-b-PS_{4600}/PEG_{5000}-b-$PMMA_{8700}$ grown at T_c = 32 °C (the maximum z-scale is 5 nm), height variance: 4.90 nm (c); four-patched surface morphology of PEG_{5000}-b-PS_{4600}/PEG_{5000}-b-$PMMA_{13100}$ grown at T_c = 30 °C (the maximum z-scale is 5 nm), height variance: 3.62 nm (d); narrow channel-wire surface morphology of PEG_{5000}-b-PS_{10000}/PEG_{5000}-b-$PMMA_{17100}$ grown at T_c = 30 °C (the maximum z-scale is 5 nm), height variance: 4.80 nm (e); broad channel-wire surface morphology of PEG_{5000}-b-PS_{10000}/PEG_{5000}-b-$PMMA_{13100}$ grown at T_c = 23 °C (the maximum z-scale is 5 nm), height variance: 5.22 nm (f). The weight ratio of PEG-b-PS/PEG-b-PMMA diblock copolymers was 50/50 for cocrystallization of all samples.

grown at T_c = 23 °C. When the molecular weights of PS and PMMA blocks were constant in 14800 and 17100 g/mol and the growth conditions were fixed, irrespective of shape and size of disperses in both morphologies, the total thicknesses in PS and PMMA covered regions were about 18.40 and 12.30 nm, respectively (the error percentage was below 3%). Consequently, the thicknesses of the crystalline and amorphous parts were 4.06 and 2.72 nm as well as 7.17 and 4.79 nm, respectively. These figures are valid for all other single crystals with special and random morphologies. In more details, for given molecular weights of PS and PMMA brushes, either PMMA's were dispersed in PS-matrix with any shape and size or they were spread with nearly 50/50 proportion in PS-PMMA channel-wire morphologies, the thicknesses were somehow equal in respective phase regions (again, the error percentage was below 3-4%). Moreover, for samples in which the molecular weights of one type of brush were similar but those of the other ones were not the thicknesses for the regions covered with brushes having the same molecular weight were equal with each other (the error percentage was below 5%). Quantitatively, the total, substrate, and amorphous thicknesses as well as tethering density for mixed-brush single crystals of PEG_{5000}-*b*-PS_{10000}/PEG_{5000}-*b*-$PMMA_{13100}$ and PEG_{5000}-*b*-PS_{4600}/PEG_{5000}-*b*-$PMMA_{13100}$ grown at T_c = 30 °C, were 18.23 and 16.12 nm, 5.47 and 7.74 nm, 6.38 and 4.18 nm, 0.408 and 0.577 cm^{-2} for PS phase regions, and similarly were 12.51 and 12.48 nm, 3.39 and 3.37 nm, 4.58 and 4.54 nm, 0.253 and 0.251 cm^{-2} for PMMA phase regions. In these two samples, due to the fixed molecular weight of PMMA

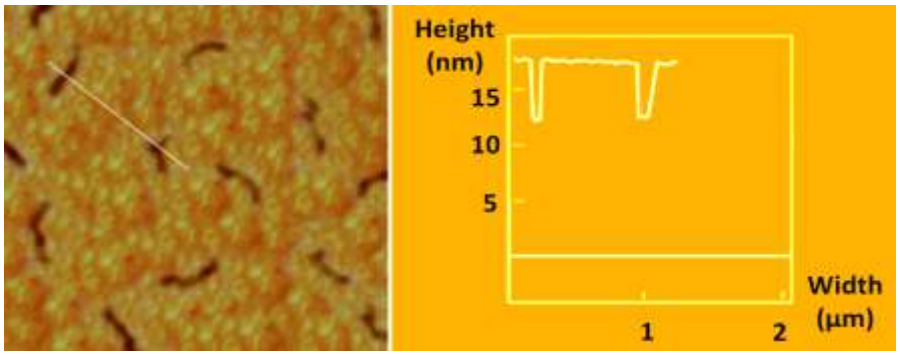

(a)

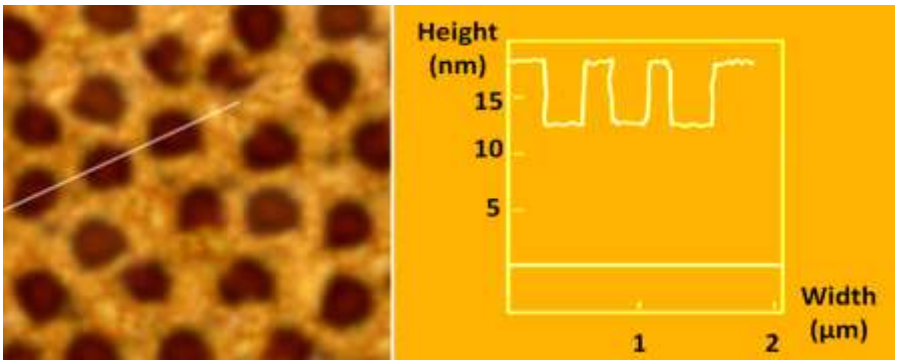

(b)

Fig. 2: AFM Nanoscope images of mixed-brush single crystals. Snake-like surface morphology of PEG_{5000}-b-PS_{14800}/PEG_{5000}-b-$PMMA_{17100}$ (grown at T_c = 23 °C), left: height image (the maximum z-scale is 5 nm), height variance: 6.10 nm, right: height profile (a); leopard skin-like surface morphology of PEG_{5000}-b-PS_{14800}/PEG_{5000}-b-$PMMA_{17100}$ (grown at T_c = 23 °C), left: height image (the maximum z-scale is 5 nm), height variance: 6.15 nm, domain size: 286 nm, right: height profile (b). The weight ratio of PEG-b-PS/PEG-b-PMMA diblock copolymers was 50/50 for cocrystallization of all samples.

tethered chains (= 13100 g/mol), the characteristics of regions covered with them proved each other, regardless of molecular weight of brushes in the neighboring phase as well as shape and size of disperses. For single crystals possessing special and random surface morphologies, in which PS brushes were matrix and PMMA tethered chains were disperses, a meaningful variance was observed in the size and length of disperses in parallel with the alterations of amorphous blocks molecular weight. For example, in morphologies having alternate channel-wire patterns, via increasing the PS and PMMA blocks molecular weight, the width of channels decreased. Furthermore, for morphologies, in which the PMMA covered areas having snake shape were spread in the PS-matrix, via enhancing the molecular weight of amorphous chains, the average length of snakes decreased. In these systems, the PMMA average domain size had a decreasing trend with molecular weight enhancement [43]. Besides, in the epitaxial structures fabricated by our research group, for channels patterned with matrix-dispersed morphologies, a similar trend was also detected for the PMMA disperses. Another elegant trend discovered in our empirical trials was the reduction of the average domain size of PEG-disperses in PS- and PMMA-matrix in cocrystallization of homo (PEG) and PEG-*b*-PS as well as PEG-*b*-PMMA diblock copolymer chains. The reason for the formation of a limited population of special morphologies (nearly 3%) besides the 97% of patterned and regular leopard skin-like morphologies could be associated with high PDI in growth systems. Due to the range of variety of amorphous blocks length, they may have more opportunities to be included in different morphologies of growing single crystals. The morphologies, in which

the portion of PMMA chains on the single crystal was less than that in ideal and patterned mixed-brush morphologies, actually possessed the longer amorphous blocks. Therefore, this phenomenon diminished the number of chains having higher hindrance. The longer PMMA chains played a more significant role; because they had packed pancake conformation due to their presence in partially poor solvent and their attractive interaction with PEG substrate. That is why, upon entering into the single crystal structure, the osmotic pressure against the similar tethers increased; because the amorphous tethered chains to prepare their demanded surface area to occupy caused the PEG crystallizable chains to have more foldings. On the other hand, via enhancement of the PS chains length, the osmotic pressure and steric repulsion for the presence of other chains also increased. Here, the hindrance against the PS stretched chains was less than that of the PMMA grafts, thereby the system preferred to further absorb the PS chains and, consequently, they developed the matrix phase. Irrespective of some scarce surface morphologies, in which the portion of PS and PMMA chains was equal on the single crystal surface (random channel-wire morphologies having alternative channels), in most of morphologies (possessing either ideal and predictable inside-filled circle disperses or ring-, dumbbell-, and snake-like patches) the portion of PS brushes on the surface of single crystal was higher than that of PMMA ones. It could be ascribed to packed pancake conformation of PMMA brushes and, consequently, their higher steric repulsion. We predict that at 23-32 °C, even in good and poor solvents for the PMMA and PS blocks, respectively, due to a dominant effect of the attractive interaction between the PMMA brushes and PEG substrate surface, they would have more packed conformation in comparison to PS ones [57]. Hence, more percentage of diblock copolymers having the PS block will be able to be included in the single crystal structure and, subsequently, be part of the matrix phase. Even in an inverse growth condition, the domination of the PS chains population will be beyond question, and they are capable of being a matrix in over 99% of the fabricated surface morphologies. Furthermore, for preparing convenient analyses condition to detect the various phase regions in mixed-brushes, the molecular weight of PMMA chains was high in comparison to that of PS ones. In addition to conformation, the longer chains of PMMA blocks could, in turn, elevate the osmotic pressure.

In the channel-like single crystals, the central channel covered by the PS and PMMA mixed-brushes was in the role of seed (core), and the outer layer was composed of PMMA homo brush single crystal. It could be related to different interactions of tethered chains with the substrate surface. Besides all experimental parameters such as solvent quality and molecular weight, the interaction dictates the conformation [57]. We speculate that in some morphologies with infinitesimal or snake-like disperses, the PMMA brushes were longer; because the growth center tended to decrease the hindrance of similar chains. In simple words, in inside-filled PMMA-disperses, the hindrance of PMMA chains against each other was higher than that of extended or hollow ones; because, in the latter ones, the border line between PMMA and PS tethered chains were longer and it could, in turn, reduce the hindrance.

By comparing the SAED patterns obtained for predictable leopard skin-like and special morphologies, it was concluded that they were to some extent similar. Either the PMMA brushes regularly and controllably were patterned in the PS-matrix or irregularly and unpredictably were dispersed in the same matrix, the growth fronts and their priority were the same; because the diblock copolymers possessed the same crystalline blocks. In conclusion, the surface morphology and the type of amorphous brushes and their molecular weight had no impact on the structure of crystalline substrate and (120) growth fronts. Figs. 3(a) and (b) illustrate *the scanning* transmission electron microscopy (*STEM*) image of PEG_{5000}-*b*-PS_{4600}/PEG_{5000}-*b*-$PMMA_{8700}$ single crystals grown in amyl acetate at T_c = 28 °C and the scheme of various surface patterning in PEG-*b*-PS/PEG-*b*-PMMA single crystals. For PEG_{5000}-*b*-PS_{4600}/PEG_{5000}-*b*-$PMMA_{8700}$ mixed-brush single crystals whose SAED patterns are illustrated in Fig. 3(c) and (d), the dominant fronts for both patterned matrix-dispersed and special morphologies were (120) prisms. Besides (120) dominant growth fronts, (110) and (020) weak spots were also detected. In these types of brush-covered nanostructures, the PS and PMMA grafted chains were categorized as disordered brushes; because, in the SAED patterns, only the spots of crystalline PEG substrate were detected. Similar results were reported in our previous works [58,59].

Ordered coily and rod brush-covered nanostructured single crystals

When PEG_{5000}-*b*-PCL_{4700}/PEG_{5000}-*b*-PS_{18500} single crystals were grown as another type of mixed-brush

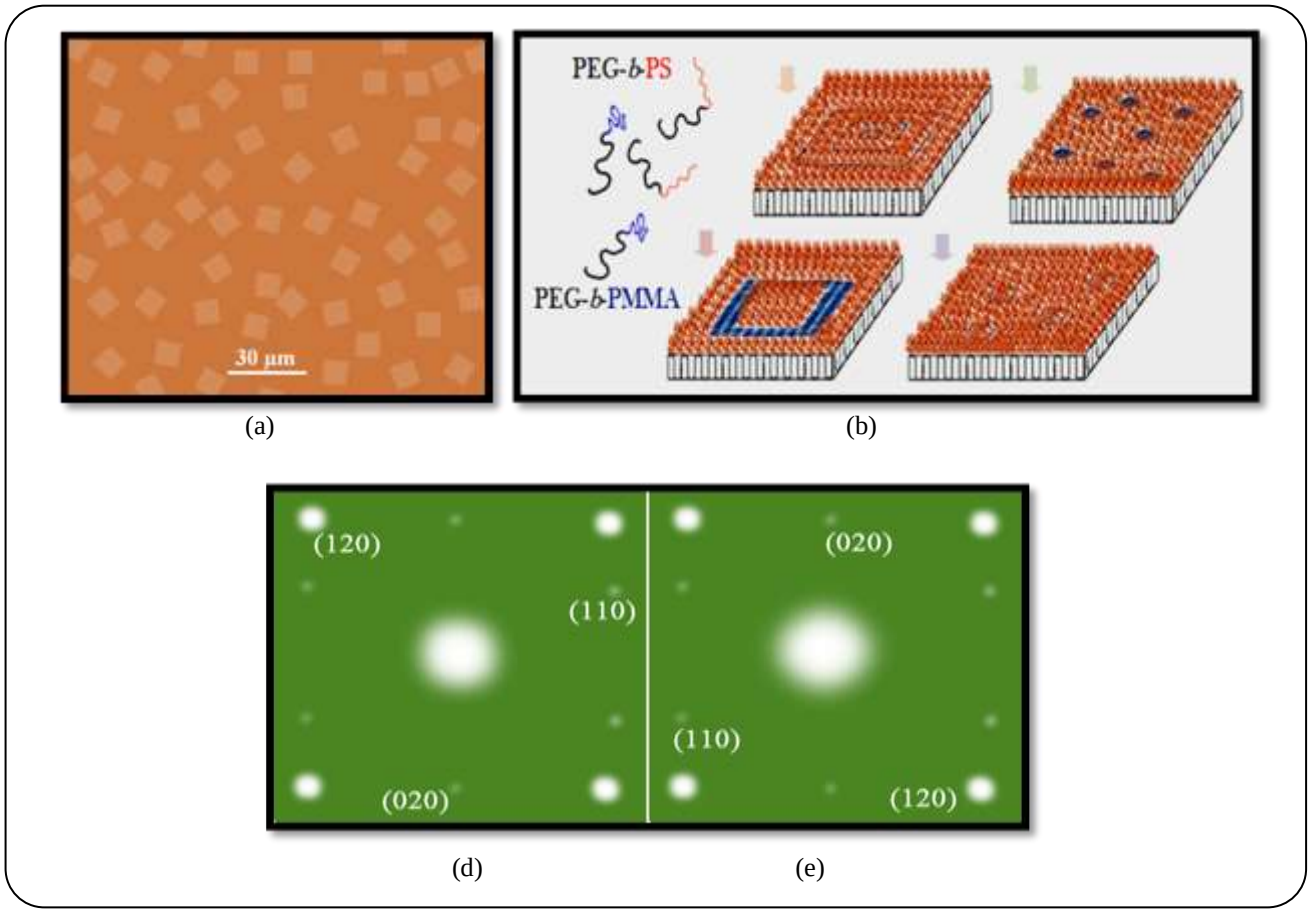

Fig. 3: (a) STEM image of PEG_{5000}-b-PS_{4600}/PEG_{5000}-b-$PMMA_{8700}$ single crystals grown in amyl acetate at T_c = 28 °C; (b) the scheme of various surface patterning in PEG-b-PS/PEG-b-PMMA single crystals; electron diffraction patterns of single crystals with random surface morphology (c) and matrix-dispersed surface morphology (d). The weight ratio of PEG-b-PS/PEG-b-PMMA diblock copolymers was 50/50 for cocrystallization of both samples.

single crystals from molten thin films, a co-continuous surface morphology was acquired. In these types of mixed-brush single crystalline grains, the grafted brushes also demonstrated an ordered structure in the SAED patterns. Figs. 4(a-c) depict STEM image of PEG_{5000}-*b*-PCL_{4700}/PEG_{5000}-*b*-PS_{18500} single crystals grown from melt state at T_c = 28 °C and the corresponding surface morphology and SAED pattern. In SAED pattern, (120) growth planes were for the crystalline PEG substrate, and (110) and (200) spots stood for the PCL ordered epitaxially grown structures on the PEG substrate. In these types of nanostructures, the characteristics of developed grains were directly measured using SAXS analyses. Because Equations (1) and (2) did not satisfy the condition of crystalline PCL brushes. The height variance between the crystalline PCL ($d^{overall}_{PCL}$ = 22.61 nm, d^{PEG}_{PCL} = 10.93 nm, d^{PCL}_{PCL} = 5.84 nm) and amorphous PS ($d^{overall}_{PS}$ = 46.56 nm, d^{PEG}_{PS} = 8.69 nm, d^{PS}_{PS} = 18.93) brushes was 23.95 nm. Therefore, the distinction between various kinds of nano-brush phases was easily possible.

Different parts of Fig. 5 depict STEM image of $PANI_{16520}$-*b*-PEG_{35000}-*b*-$PANI_{16520}$ single crystals grown from the melt state at T_c = 18 °C, the corresponding dispersed-dispersed surface morphology, and AFM phase image. Based on AFM height profile and AFM ImageJ software, the PANI nanofiber diameter ranged from 6 to 8 nm. In AFM phase image of PANI nanorod-covered single crystals, the whole surface of single crystal was in a united phase. In the Interface Distribution Function (IDF) of SAXS, the first peak stood for the thickness of the crystalline substrate (d^{PEG}_{PANI} = 4.85 nm) and the second peak indicated the twice of the thickness of PANI brushes ($2d^{PANI}_{PANI}$ = 298.02 nm). Although the PANI nanorods

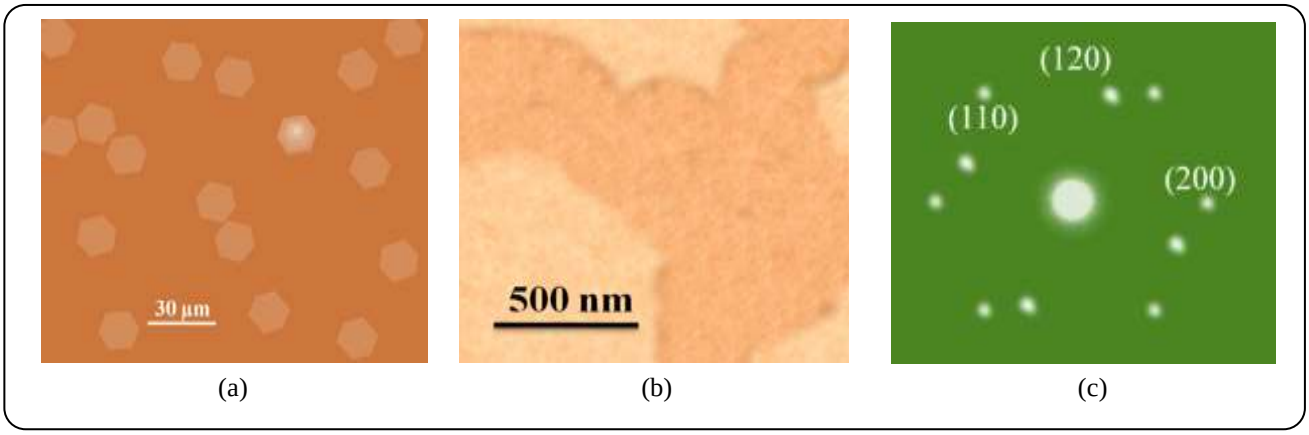

Fig. 4: (a) STEM image of PEG_{5000}-b-PCL_{4700}/PEG_{5000}-b-PS_{18500} single crystal grown from melt at T_c = 28 °C; (b) the corresponding surface morphology and (c) SAED pattern; $d^{overall}_{PCL}$ = 22.61 nm, d^{PEG}_{PCL} = 10.93 nm, d^{PCL}_{PCL} = 5.84 nm; $d^{overall}_{PS}$ = 46.56 nm, d^{PEG}_{PS} = 8.69 nm, d^{PS}_{PS} = 18.93.

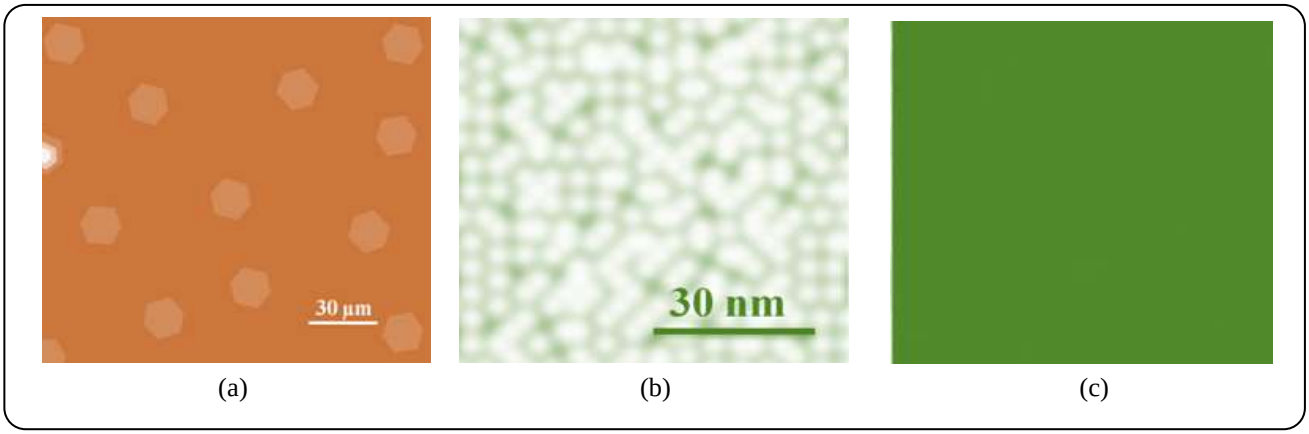

Fig. 5: STEM image of $PANI_{16520}$-b-PEG_{35000}-b-$PANI_{16520}$ single crystals grown from the melt at T_c = 18 °C; the corresponding (b) AFM dispersed-dispersed surface morphology and (c) phase image; $d^{overall}_{PANI}$ = 302.87, d^{PEG}_{PANI} = 4.85 nm, d^{PANI}_{PANI} = 149 nm, PANI fiber diameter range = 6-8 nm.

were not crystallizable, their arrangement on the PEG single crystals was categorized as the ordered brushes; because they were fully extended and orderly arranged in the vicinity of each other. Here, the thickness of the PEG substrate did not vary by an increase of PANI molecular weight. This was due to the extended conformation of PANI brushes on the PEG_{35000} substrates. By lengthening the PANI nanofibers, their exerted osmotic pressure onto the substrate surface did not change, and from the beginning, only PANI nanofibers having too small diameters have been allowed to be entered into the single crystals.

CONCLUSIONS

Various ordered and disordered polymer nano-brushes with distinct surface morphologies were developed through the growth of single crystals from dilute solution and thin molten films comprising PEG-*b*-PS and PEG-*b*-PMMA, PEG-*b*-PCL, and PANI-*b*-PEG-*b*-PANI block copolymers. The features of PS/PMMA covered mixed-brush single crystals including the surface of various PS- and PMMA-covered phases, the total, substrate, and amorphous thicknesses resembled that of patterned morphologies. The PS and PMMA nano-brushes were categorized in disordered brushes; however, the PCL and PANI ones were grouped in ordered brushes. The characteristics of grown single crystals such as surface morphology, growth planes, and thicknesses were investigated using AFM, SAED, and SAXS analyses.

Received : Sep. 14, 2016 ; Accepted : Oct. 16, 2017

REFERENCES

[1] Li B., Wang B., Ferrier Jr. R.C., Li C.Y., Programmable Nanoparticle Assembly *via* Polymer Single Crystals, *Macromolecules*, **42**: 9394-9399 (2009).

[2] Chen X., Wang W., Cheng S., Dong B., Li C. Y., Mimicking Bone Nanostructure by Combining Block Copolymer Self-assembly and 1D Crystal Nucleation, *ACS Nano*, **7**: 8251-8257 (2013).

[3] Chen W. Y., Zheng J. X., Cheng S. Z. D., Li C. Y., Huang P., Zhu L., Xiong H., Ge Q., Guo Y., Quirk R. P., Lotz B., Deng L., Wu C., Thomas E. L., Onset of Tethered Chain Overcrowding, *Phys. Rev. Lett.*, **93**: 028301-1 (2004).

[4] Chen W. Y., Li C. Y., Zheng J. X., Huang P., Zhu L., Ge Q., Quirk R. P., Lotz B., Deng L., Wu C., Thomas E. L., Cheng S. Z. D., Chemically Shielded Poly(ethylene oxide) Single Crystal Growth and Construction of Channel-Wire Arrays with Chemical and Geometric Recognitions on a Submicrometer Scale, *Macromolecules*, **37**; 5292-5299 (2004).

[5] Li B., Li L. Y., Wang B. B., Li C.Y., Alternating Patterns on Single-Walled Carbon Nanotubes, *Nat. Nanotechnol.*, **4**: 358-362 (2009).

[6] Li C.Y., Polymer Single Crystal Meets Nanoparticles, *J. Polym. Sci., Part B: Polym. Phys.*, **47**: 2436-2440 (2009).

[7] Dong B., Miller D. L., Li C. Y., Polymer Single Crystal as Magnetically Recoverable Support for Nanocatalysts, *J. Phys. Chem. Lett.*, **3**: 1346-1350 (2012).

[8] Li B., Li C. Y., Immobilizing Au Nanoparticles with Polymer Single Crystals, Patterning and Asymmetric Functionalization, *J. Am. Chem. Soc.*, **129**: 12-13 (2007).

[9] Wang B. B., Li B., Dong B., Zhao B., Li C. Y., Homo- and Hetero-Particle Clusters Formed by Janus Nanoparticles with Bicompartment Polymer Brushes, *Macromolecule*, **43**: 9234-9238 (2010).

[10] Fujiki Y., Tokunaga N., Shinkai S., Sada K., Anisotropic Decoration of Gold Nanoparticles onto Specific Crystal Faces of Organic Single Crystals, *Angew. Chem., Int. Ed.*, **45**: 4764-4767 (2006).

[11] Minemawari H., Yamada T., Matsui H., Tsutsumi J., Haas S., Chiba R., Kumai R., Hasegawa T., Inkjet Printing of Single-Crystal Films, *Nature*, **475**: 364-367 (2011).

[12] Kim D. H., Han J. T., Park Y. D., Jang Y., Cho J. H., Hwang M., Cho, K., Single-Crystal Polythiophene Microwires Grown by Self-Assembly, *Adv. Mater.*, **18**: 719-723 (2006).

[13] Jiang X., Liu X., Liao Q., Wang X., Yan D. D., Huo H., Li L., Zhou J. J., Probing Interfacial Properties Using a Poly(ethylene oxide) Single Crystal, *Soft Matter*, **10**: 3238-3244 (2014).

[14] Di Bonito P., Petrone L., Casini G., Francolini I., Ammendolia M. G., Accardi L., Piozzi A., D'Ilario L., Martinelli A., Amino-Functionalized Poly(L-lactide) Lamellar Single Crystals as a Valuable Substrate for Delivery of hPV16-e7 Tumor Antigen in Vaccine Development, *Int. J. Nanomedicine*, **10**: 3447 (2015).

[15] D'Ilario L., Francolini I., Martinelli A., Piozzi A., Dipyridamole-Loaded Poly (L-lactide) Single Crystals as Drug Delivery Systems, *Macromol. Rapid Commun.*, **28**: 1900-1904 (2007).

[16] Petrone L., Ammendolia M. G., Cesolini A., Caimi S., Superti F., Giorgi C., Di Bonito P., Recombinant HPV16 E7 Assembled into Particles Induces an Immune Response and Specific Tumour Protection Administered without Adjuvant in an Animal Model, *J. Transl. Med.*, **9**: 69 (2011).

[17] Dong B., Zhou T., Zhang H., Li C. Y., Directed Self-Assembly of Nanoparticles for Nanomotors, *ACS Nano*, **7**: 5192-5198 (2013).

[18] Liu M., Liu L., Gao W., Su M., Ge Y., Shi L., Zhang H., Dong B., Li C. Y., A Micromotor Based on Polymer Single Crystals and Nanoparticles: Toward Functional Versatility, *Nanoscale*, **6**: 8601-8605 (2014).

[19] Rahimi K., Botiz I., Stingelin N., Kayunkid N., Sommer M., Koch F. P., Nguyen H., Coulembier O., Dubois P., Brinkmann M., Reiter, G., Controllable Processes for Generating Large Single Crystals of Poly(3-hexylthiophene), *Angew. Chem., Int. Ed.*, **51**: 11131-11135 (2012).

[20] Hourani W., Rahimi K., Botiz I., Koch F. P. V., Reiter G., Lienerth P., Heiser T., Bubendorff J. L., Simon L., Anisotropic Charge Transport in Large Single Crystals of π-Conjugated Organic Molecules, *Nanoscale*, **6**: 4774-4780 (2014).

[21] Dong H., Jiang S., Jiang L., Liu Y., Li H., Hu W., Wang E., Yan S., Wei Z., Xu W., Gong X., Nanowire Crystals of a Rigid Rod Conjugated Polymer, *J. Am. Chem. Soc.*, **131**: 17315-17320 (2009).

[22] Goto H., Okamoto Y., Yashima E., Solvent-Induced Chiroptical Changes in Supramolecular Assemblies of an Optically Active, Regioregular Polythiophene, *Macromolecules*, **35**: 4590-4601 (2002).

[23] Ma Z., Geng Y., Yan D., Extended-chain Lamellar Packing of Poly (3-butylthiophene) in Single Crystals, *Polymer*, **48**: 31-34 (2007).

[24] Kim D. H., Park Y. D., Jang Y., Yang H., Kim Y. H., Han J. I., Moon D. G., Park S., Chang T., Chang C., Joo M., Ryu C. Y., Cho, K., Enhancement of Field-Effect Mobility Due to Surface-Mediated Molecular Ordering in Regioregular Polythiophene Thin Film Transistors, *Adv. Funct. Mater.*, **15**: 77-82 (2005).

[25] Kim D. H., Park Y. D., Jang Y., Cho, K., Solvent Vapor-Induced Nanowire Formation in Poly (3-hexylthiophene) Thin Films, *Macromol. Rapid Commun.*, **26**: 834-839 (2005).

[26] Xiao X., Hu Z., Wang Z., He T., Study on the Single Crystals of Poly(3-octylthiophene) Induced by Solvent-Vapor Annealing, *J. Phys. Chem. B*, **113**: 14604-14610 (2009).

[27] Harris B. P., Kutty J. K., Fritz E. W., Webb C. K., Burg K. J. L., Metters A. T., Photopatterned Polymer Brushes Promoting Cell Adhesion Gradients, *Langmuir*, **22**: 4467-4471 (2006).

[28] Minko S., Patil S., Datsyuk V., Simon F., Eichhorn K.J., Motornov M., Usov D., Tokarev I., Stamm M., Synthesis of Adaptive Polymer Brushes *via* "Grafting to" Approach from Melt, *Langmuir*, **18**: 289-296 (2002).

[29] Kim J.U., Matsen M.W., Finite-Stretching Corrections to the Milner-Witten-Cates Theory for Polymer Brushes, *Eur. Phys. J. E.*, **23**: 135-144 (2007).

[30] Rouhi A.M., Contemporary Biomaterials, *Chem. Eng. News*, **77**: 51 (1999).

[31] Niklason L. E., Gao J., Abbott W. M., Hirschi K. K., Houser S., Marini R., Langer R., Functional Arteries Grown In Vitro, *Science*, **284**: 489-493 (1999).

[32] Minko S., Usov D., Motornov M., Ionov L., Stamm M., Smart Responsive Interface, *Polym. Mater. Sci. Eng.*, **89**: 156 (2003).

[33] Zhao B., Synthesis of Binary Mixed Homopolymer Brushes by Combining Atom Transfer Radical Polymerization and Nitroxide-Mediated Radical Polymerization, *Polymer*, **44**: 4079-4083 (2003).

[34] Ionov L., Zdyrko B., Sidorenko A., Minko S., Klep V., Luzinov I., Stamm M., Gradient Polymer Layers by "Grafting to" Approach, *Macromol. Rapid Commun.*, **25**: 360-365 (2004).

[35] Johnson P. A., Gaspar M. A., Levicky R., Polymer-Anchored DNA Gene Monolayers, *J. Am. Chem. Soc.*, **126**: 9910-9911 (2004).

[36] Nakashima H., Furukawa K., Ajito K., Kashimura Y., Torimitsu K., Selective Chemisorption of End-Functionalized Conjugated Polymer on Macro- and Nanoscale Surfaces, *Langmuir*, **21**: 511-515 (2005).

[37] Jordan R., Ulman A., Kang J. F., Rafailovich M. H., Sokolov, J., Surface-Initiated Anionic Polymerization of Styrene by Means of Self-Assembled Monolayers, *J. Am. Chem. Soc.*, **121**: 1016-1022 (1999).

[38] de Bore B., Simon H. K., Werts M. P. L., van der Vegte E. W., Hadziioannou G., Living Free Radical Photopolymerization Initiated from Surface-Grafted Iniferter Monolayers, *Macromolecules*, **33**: 349-356 (2000).

[39] Weimer M. W., Chen H., Giannelis E. P., Sogah D. Y., Direct Synthesis of Dispersed Nanocomposites by In Situ Living Free Radical Polymerization Using a Silicate-Anchored Initiator, *J. Am. Chem. Soc.*, **121**: 1615-1616 (1999).

[40] Matyjaszewski K., Miller P. J., Shukla N., Immaraporn B., Gelman A., Luokala B. B., Siclovan T.M., Lickelbick G., Vallant T., Hoffmann H., Pakula, T., Polymers at Interfaces: Using Atom Transfer Radical Polymerization in the Controlled Growth of Homopolymers and Block Copolymers from Silicon Surfaces in the Absence of Untethered Sacrificial Initiator, *Macromolecules*, **32**: 8716-8724 (1999).

[41] Weck M., Jackiw J. J., Rossi R. R., Weiss P. S., Grubbs R.H., Ring-Opening Metathesis Polymerization from Surfaces, *J. Am. Chem. Soc.*, **121**: 4088-4089 (1999).

[42] Zheng J. X., Xiong H., Chen W.Y., Lee K., Van Horn R. M., Quirk R. P., Lotz B., Thomas E. L., Shi A.C., Cheng, S.Z.D., Onsets of Tethered Chain Overcrowding and Highly Stretched Brush Regime *via* Crystalline-Amorphous Diblock Copolymers, *Macromolecules*, **39**: 641-650 (2006).

[43] Abbaspoor S., Abbasi F., Agbolaghi S., A Novel Approach to Prepare Polymer Mixed-Brushes via Single Crystal Surface Patterning, *RSC Adv.*, **4**: 17071-17082 (2014).

[44] Agbolaghi S., Alizadeh-Osgouei M., Abbaspoor S., Abbasi F., Self-Assembling Nano Mixed-Brushes Having Co-continuous Surface Morphology by Melt Growing Single Crystals and Comparison with Solution Patterned Leopard-Skin Surface Morphology, *RSC Adv.*, **5**: 1538-1548 (2015).

[45] Agbolaghi S., Abbasi F., Abbaspoor S., Alizadeh-Osgouei M., Self-Designed Surfaces via Single-co-Crystallization of Homopolymer and Diblock Copolymers in Various Growth Conditions, *Eur. Polym. J.*, **66**: 108-118 (2015).

[46] Agbolaghi S., Abbasi, F., Abbaspoor S., Epitaxial Single Crystal Surface Patterning and Study of Physical and Chemical Environmental Effects on Crystal Growth, *Colloid Polym. Sci.*, **292**: 1375-1383 (2014).

[47] Nazari M., Agbolaghi S., Abbaspoor S., Gheybi H., Abbasi F., Arrangement of Conductive Rod Nanobrushes *via* Conductive–Dielectric–Conductive Sandwiched Single Crystals of Poly(ethylene glycol) and Polyaniline Block Copolymers, *Macromolecules*, **48**: 8947-8957 (2016).

[48] Agbolaghi S., Nazari M., Abbaspoor S., Gheybi H., Abbasi F., Micro/Nano Conductive-Dielectric Channels Designed by Poly(ethylene glycol) Single Crystals Covered by Polyaniline Nanofibers, *Polymer*, **92**: 264-272 (2016).

[49] Agbolaghi S., Nazari M., Abbaspoor S., Gheybi H., Abbasi F., Characterization of Novel Extremely Extended Regime in Conductive Rod-Like Polyaniline Nanobrush-Covered Poly(ethylene glycol) Single Crystals, *Eur. Polym. J.*, **82**: 196-207 (2016).

[50] Alizadeh-Osgouei M., Agbolaghi S., Abbaspoor S., Abbasi F., A Subtle Insight into Nano-Convergence of Substrate Thickness in Melt-grown Single-co-Crystals, *Colloid Polym. Sci.*, **294**: 869-878 (2016).

[51] Lotz B., Kovacs A. J., Propriétés des Copolymères Biséquencés Polyoxyéthylène-Polystyrène, *Colloid Polym. Sci.*, **209**: 97-114 (1966).

[52] Lotz B., Kovacs A. J., Bassett G. A., Keller A., Properties of Copolymers Composed of One Poly-ethylene-oxide and One Polystyrene Block, *Colloid Polym. Sci.*, **209**: 115-128 (1966).

[53] Brandup J., Immergut E. H., "Polymer Handbook", John Wiley & Sons, Inc., New York (1975).

[54] Xiong H., Zheng J. X., Van Horn R. M., Jeong K. U, Quirk R. P., Lotz B., Thomas E. L., Brittain W. J., Cheng S. Z. D., A New Approach in the Study of Tethered Diblock Copolymer Surface Morphology and Its Tethering Density Dependence, *Polymer*, **48**: 3732-3738 (2007).

[55] Bhushan B., Israelachvili J. N., Landman U., Nanotribology: Friction, Wear and Lubrication at the Atomic Scale, *Nature*, **374**: 607-616 (1995).

[56] Wunderlich B., "Macromolecular Physics", Vol. 1: Crystal Structure, Morphology, Defects, Academic, New York (1973).

[57] Abbaspoor S., Abbasi F., Agbolaghi S., Effects of Various Polymer Brushes on the Crystallization of Poly(ethylene glycol) in Poly(ethylene glycol)-*b*-polystyrene and Poly(ethylene glycol)-*b*-poly(methyl methacrylate) Single Crystals. *J. Polym. Res.*, **21**: 493 (1-8) (2014).

[58] Agbolaghi S., Abbasi F., Abbaspoor S., Preparation of Polymer Brushes via Growth of Single Crystals of Poly(ethylene glycol)-*block*-Polystyrene Diblock Copolymers Synthesized by ATRP and Studying the Crystal Lateral Size and Brush Tethering Density, *Polym. Bull.*, **71**: 3177-3196 (2014).

[59] Agbolaghi S., Abbasi F., Jalili K., Nascent Lateral Habits of Solution Crystallization of Poly(ethylene glycol)-*block*-polystyrene Diblock Copolymers, *J. Polym. Res.*, **21**: 380 (1-11) (2014).